

On the Energy Spectra of GeV/TeV Cosmic Ray Leptons

Lukasz Stawarz^{1,2}, Vahé Petrosian^{1,3}, & Roger D. Blandford¹

stawarz@slac.stanford.edu

ABSTRACT

Recent observations of cosmic ray electrons from several instruments have revealed various degrees of deviation in the measured electron energy distribution from a simple power-law, in a form of an excess around 0.1 to 1 TeV energies. An even more prominent deviation and excess has been observed in the fraction of cosmic ray positrons around 10 and 100 GeV energies. These observations have received considerable attention and many theoretical models have been proposed to explain them. The models rely on either dark matter annihilation/decay or specific nearby astrophysical sources, and involve several additional assumptions regarding the dark matter distribution or particle acceleration. In this paper we show that the observed excesses in the electron spectrum may be easily reproduced without invoking any unusual sources other than the general diffuse Galactic components of cosmic rays. The model presented here assumes a power-law injection of electrons (and protons) by supernova remnants, and evaluates their expected energy spectrum based on a simple kinetic equation describing the propagation of charged particles in the interstellar medium. The primary physical effect involved is the Klein-Nishina suppression of the electron cooling rate around TeV energies. With a very reasonable choice of the model parameters characterizing the local interstellar medium, we can reproduce the most recent observations by Fermi and HESS experiments. Interestingly, in our model the injection spectral index of cosmic ray electrons becomes comparable to, or even equal to that of cosmic ray protons. The Klein-Nishina effect may also affect the propagation of the secondary e^\pm pairs, and therefore modify the cosmic ray positron-to-electron ratio. We have explored this possibility by considering two mechanisms for production of e^\pm pairs within the Galaxy. The first is due to the decay of π^\pm 's produced by interaction of cosmic ray nuclei with ambient

¹Kavli Institute for Particle Astrophysics and Cosmology, Stanford University, Stanford CA 94305, USA

²Astronomical Observatory of the Jagiellonian University, ul. Orła 171, 30-244 Kraków, Poland

³Departments of Physics and of Applied Physics, Stanford University, Stanford CA 94305, USA

protons. The second source discussed here is due to the annihilation of the diffuse Galactic γ -rays on the stellar photon field. We find that high positron fraction increasing with energy, as claimed by the PAMELA experiment, cannot be explained in our model with the conservative set of the model parameters. We are able, however, to reproduce the PAMELA (as well as Fermi and HESS) results assuming high values of the starlight and interstellar gas densities, which would be more appropriate for vicinities of supernova remnants. A possible solution to this problem may be that cosmic rays undergo most of their interactions near their sources due to the efficient trapping in the far upstream of supernova shocks by self-generated, cosmic ray-driven turbulence.

Subject headings: cosmic rays — Galaxy: general — ISM: general

1. Introduction

Measurements of the energy spectra of cosmic ray (CR) species are of a great importance for understanding the physics of Galactic CR sources (such as pulsars or supernova remnants), as well as for constraining the internal structure of Milky Way, since this structure (topology and intensity of the Galactic magnetic field, profiles and energy distribution of different Galactic photon fields, distribution of interstellar gas and dust, etc.) determines the spatial and energy evolution of the injected charged particles which propagate through the interstellar medium. In addition, as discussed in several papers by a number of authors (e.g., Jungman et al. 1996; Cheng et al. 2002), annihilation or decay of a dark matter (Kaluza-Klein particles or supersymmetric WIMPs) may also imprint some signatures in the observed spectra of CR electrons within the GeV–TeV energy range. Consequently, the most recent observations by the ATIC, PAMELA, Fermi, and HESS experiments (Chang et al. 2008; Adriani et al. 2009; Abdo et al. 2009; Aharonian et al. 2008, 2009a, respectively) have generated significant interest on this topic in astrophysics and particle physics communities.

The most sophisticated framework for analyzing the CR propagation within the Galaxy is provided by the GALPROP model presented first by Moskalenko & Strong (1998) and Strong & Moskalenko (1998). This model assumes injection of a power-law electrons and nuclei, and follows their spatial and energy evolution under the influence of different radiative processes (Coulomb losses, synchrotron and IC cooling, proton-proton collisions, etc.), taking also into account the relevant interactions of charged particles with the interstellar turbulent magnetic field (with the assumed Kolmogorov spectrum) in a quasi-linear approximation regime. The model can successfully explain many findings regarding the hadronic CR spectrum and its composition (Moskalenko et al. 2002, 2003), as well as the observed Galac-

tic diffuse γ -ray emission (Moskalenko & Strong 2000; Strong et al. 2000, 2004; Porter et al. 2008). However, the model predicts also the decrease of the CR positron-to-electron ratio with particles' energy in the GeV–TeV range, in a disagreement with the observational indications. This prediction was made under the working hypothesis that bulk of the Galactic e^\pm pairs are created in the collisions of relativistic CR protons with ambient gas, and the subsequent decays of the generated pions (see the discussion in Moskalenko & Strong 1998). One should note that the previous (prior to 2008) measurements regarding this issue were restricted to electron energies $E_e < 10$ GeV, and as such could be seriously affected by the charge dependence of solar modulation. On the other hand, the most recent PAMELA observations, reaching $E_e \simeq 100$ GeV energies, confirmed the increasing positron fraction in the CR spectrum (Adriani et al. 2009).

The other challenge to the ‘standard’ model of CR propagation came from the observations of ATIC collaboration, which reported a sharp pile-up around $E_e \simeq 0.5$ TeV above the power-law spectrum both observed at lower energies but also emerging from the GALPROP calculations (Chang et al. 2008). Reality of this sharp spectral feature has been questioned by the Fermi and HESS experiments (see Abdo et al. 2009; Aharonian et al. 2009a), which show a much smaller and broader excess over the best fit power-law continuum $J_e(E_e) \propto E_e^{-3}$. In this context one has to keep in mind that due to rapid radiative losses of the TeV-energy electrons, their spectrum measured in the Solar System may be possibly dominated by a few local sources (most likely nearby pulsars such as Vela or Geminga; see, e.g., Shen 1970; Nishimura et al. 1980; Aharonian et al. 1995; Kobayashi et al. 2004), and therefore may be more complex than a featureless power-law continuum. In particular, it may reflect the non-stationary and stochastic nature of such sources (Pohl & Esposito 1998; Grasso et al. 2009). More interestingly, the substructure around 0.5 TeV observed by ATIC was argued to be consistent with that expected from the annihilation of the Kaluza-Klein dark matter particles (Chang et al. 2008). Both ‘local pulsar’ and dark matter scenarios were claimed to successfully account for the increasing positron fraction in the CR spectrum as well (e.g., Pohl 2009; Grasso et al. 2009).

Obviously, the dark matter interpretation of the ATIC, Fermi, HESS and PAMELA results is of a great interest. However, in order to fit the collected data in the framework of this model, large though arbitrary ‘boost factors’ have to be invoked for the dark matter annihilation/decay fluxes, which are only roughly justified by a possible non-uniform (clumpy) distribution of the dark matter near the Solar System (e.g. Chang et al. 2008; Elahi et al. 2009; Hooper & Zurek 2009). In addition, as shown by Profumo & Jeltama (2009), the dark matter scenario for the positron excess conflicts with the observations of the extragalactic background radiation in the X-ray/ γ -ray energy range (see also Belikov & Hooper 2009). Similarly, the ‘local pulsar’ interpretation also relies on several model assumptions (regarding

particle acceleration in relativistic outflows), which are not observationally verified yet.

In this paper we explore the possibility of explaining the aforementioned data sets by a simple model for the generation and propagation of CRs in the Galaxy (and the vicinity of Earth), without invoking any new/unconventional sources of the TeV-energy electrons or positrons. This scenario is not intended to compete with the complexity of the GALPROP model. It is intended instead to point out several effects which, even though being standard and at some level inevitable, might have been underestimated or overlooked in the previous analysis. The new physics involved here is that we emphasize the importance of the Klein-Nishina (KN) suppression of the inverse Compton (IC) scattering cross section for ultrarelativistic electrons and positrons interacting with the Galactic starlight and other photon fields. We evaluate the modification of the primary electron energy spectrum which results from this new aspect, as well as that of secondary pairs arising from the annihilation of the Galactic γ -rays on starlight and from CR proton interactions with the interstellar medium (ISM). In §2 we discuss our model and present the kinetic equation describing the propagation of CR electrons (as well as protons and positrons). We first describe the KN effect qualitatively and then compare the CR electron spectra obtained from detailed solution of the kinetic equation with observations. In §3 we consider various mechanisms for production of secondary e^\pm pairs and derive their spectra using the same propagation model, comparing again the resulting spectra with those observed by PAMELA. A brief discussion and summary is presented in §4.

2. Primary CR Electrons

We start this section with the description of the relevant interactions of CR electrons (accelerated and injected into the Galaxy by, presumably, supernova remnants) with the ISM photons (mainly starlight), magnetic field, and turbulence. We then describe the resultant spectra of these ‘primary’ electrons and compare them with the observations reported by ATIC, Fermi, HESS, and other experiments.

2.1. Interactions of CR Electrons

The propagation of relativistic electrons injected into the ISM is determined by two basic interactions: radiative cooling and interactions with plasma turbulence. The latter causes diffusion in space (determining the rate of the escape of electrons from the Galaxy) and diffusion in energy (determining the rate of the acceleration). For the electrons with energies

above GeV, the radiative cooling is mainly via the IC scattering on ambient photon fields and due to the synchrotron emission in the Galactic magnetic field. The relevant photon fields are the Cosmic Microwave Background (CMB) radiation with the energy density $u_{cmb} \simeq 0.26 \text{ eV cm}^{-3}$, the Galactic starlight, and far infrared photons from the dust emission. The latter two are expected to dominate over the CMB (i.e., $u_{star}, u_{dust} > u_{cmb}$) in the inner parts of the Galactic disk ($r \lesssim 10 \text{ kpc}$ from the center) by a factor of at least a few (see, e.g., Strong et al. 2000; Porter et al. 2006; Moskalenko et al. 2006; Porter et al. 2008). For an electron with energy E_e , the characteristic cooling timescale in the Thomson (T) regime is therefore given as

$$\begin{aligned} \tau_{rad,T} &\simeq \frac{3 m_e^2 c^3}{4 \sigma_T u_{tot} E_e}, \quad \text{with} \\ u_{tot} &\equiv u_{cmb} (1 + \xi) + \frac{B^2}{8\pi} \quad \text{and} \quad \xi \equiv \frac{u_{dust} + u_{star}}{u_{cmb}}. \end{aligned} \quad (1)$$

From this one gets $\tau_{rad,T} \simeq 10^9 (E_e/\text{GeV})^{-1} (1 + 0.1 B_{\mu\text{G}}^2 + \xi)^{-1} \text{ yr}$, which, for the illustrative (though expected) Galactic magnetic field $B_{\mu\text{G}} \equiv B/\mu\text{G} \simeq 3$ and $\xi \simeq 10$, leads to $\tau_{rad,T} \simeq 100 (E_e/\text{GeV})^{-1} \text{ Myr}$. This estimate breaks down at high particle (and/or photon) energies where the KN effect reduces the IC cross section. This happens when the target photon energy in the electron rest frame exceeds electron rest mass, which, in the observer frame, translates to $\varepsilon > m_e^2 c^4 / 4E_e \simeq 65 (E_e/\text{GeV})^{-1} \text{ eV}$ (Blumenthal & Gould 1970).

For the evaluation of the interactions of CR electrons with magnetic turbulence we use the quasi-linear approximation for the particle-wave interactions (see, e.g., Schlickeiser 2002, and references therein) and assume a Kolmogorov spectrum of turbulence as a superposition of magnetohydrodynamical (MHD) waves. The corresponding spatial diffusion timescale may be estimated as $\tau_{esc} \simeq 3 \ell^2 / c \lambda(E_e)$, where ℓ is the linear scale of the system and the particle mean free path $\lambda(E_e) \simeq \zeta r_g^{1/3} \lambda_{max}^{2/3}$. Here $\zeta \equiv (B/\delta B)^2$ is the ratio of energy densities stored in the large-scale (‘unperturbed’) and turbulent magnetic fields, $r_g \equiv E_e/eB \simeq 3 \times 10^{12} (E_e/\text{GeV}) B_{\mu\text{G}}^{-1} \text{ cm}$ is the electron gyroradius, and λ_{max} is the maximum wavelength of the turbulent modes. This gives $\tau_{esc} \simeq 10^7 \zeta^{-1} B_{\mu\text{G}}^{1/3} (\ell/\text{kpc})^2 (\lambda_{max}/\text{kpc})^{-2/3} (E_e/\text{GeV})^{-1/3} \text{ yr}$ which, for the ISM parameters $B_{\mu\text{G}} \simeq 3$, $\zeta \simeq 1$, and $\lambda_{max} \simeq 1 \text{ kpc}$, simplifies further to $\tau_{esc} \simeq 10 (\ell/\text{kpc})^2 (E_e/\text{GeV})^{-1/3} \text{ Myr}$. In other words, an electron with energy E_e travels the distance $\ell \simeq 3 (E_e/\text{GeV})^{-1/3} \text{ kpc}$ within ISM before losing its energy via radiative cooling (for $\xi \simeq 10$). Hence, high-energy CR electrons ($E_e > 10 \text{ GeV}$) detected near the Earth are supposed to originate from local ($\ell < 3 \text{ kpc}$) region and recently operating ($t < 100 \text{ Myr}$) sources (Shen 1970).

It should be noted in this context that several observational findings (regarding, e.g., secondary-to-primary ratios of some CR elements) are better interpreted in terms of the

particle diffusion shaped by the ISM turbulence characterized by the Kraichnan energy spectrum, rather than of the Kolmogorov form anticipated above (see Ptuskin et al. 2006; Strong et al. 2007, and references therein). If this is the case indeed, then $\lambda(E_e) \simeq \zeta r_g^{1/2} \lambda_{max}^{1/2}$ and $\tau_{esc} \simeq 500 (\ell/\text{kpc})^2 (E_e/\text{GeV})^{-1/2} \text{Myr}$, and hence the conclusion regarding the local origin of $> 10 \text{ GeV}$ energy CR electrons is even strengthened.

On the other hand, the order-of-magnitude estimate presented above should be taken with caution, because of the uncertainty in the value of λ_{max} , which is not a directly measured quantity, but is only expected to be roughly of the scale of the Galactic disk thickness, $\sim 1 \text{ kpc}$. In addition, the use of the Kolmogorov/Kraichnan spectrum for ISM turbulence is only partly justified by observations/theoretical models (see, e.g., Cho et al. 2003; Strong et al. 2007, and references therein). Finally, the anticipated quasi-linear approximation is appropriate for modeling of the particle diffusion *along* the magnetic field lines (and thus rather *within* the Galactic disk), and is not expected to describe properly the propagation of particles *across* the magnetic field lines (i.e., the escape of particles from the Galactic disk).

The spatial diffusion of CR electrons is accompanied by their diffusion in the momentum space, leading to a net acceleration of particles on the characteristic timescale $\tau_{acc} \simeq 3 \lambda(E_e)/c\beta_{sc}^2$, where β_{sc} is the velocity of turbulent MHD modes in the units of speed of light (e.g., Blandford & Eichler 1987). For a low-beta plasma, the MHD wave velocity is equal to the Alfvén velocity $c\beta_{sc} \simeq v_A = B/(4\pi m_p n_{ism})^{1/2} \simeq 2 \times 10^5 B_{\mu\text{G}} (n_{ism}/\text{cm}^{-3})^{-1/2} \text{cm s}^{-1}$, where n_{ism} is the number density of the ambient plasma. Thus, for a Kolmogorov spectrum of the ISM turbulence $\tau_{acc} \simeq 10^{11} \zeta B_{\mu\text{G}}^{-7/3} (\lambda_{max}/\text{kpc})^{2/3} (n_{ism}/\text{cm}^{-3}) (E_e/\text{GeV})^{1/3} \text{yr}$. Assuming again values $B_{\mu\text{G}} \simeq 3$, $\zeta \simeq 1$, $\lambda_{max} \simeq 1 \text{ kpc}$, and $n_{ism} \simeq 1 \text{ cm}^{-3}$, this simplifies further to $\tau_{acc} \simeq 10^4 (E_e/\text{GeV})^{1/3} \text{Myr}$, which indicates that ultrarelativistic electrons undergo little turbulent acceleration within ISM before they cool radiatively or escape (see in this context, e.g., Ptuskin et al. 2006). Thus, radiative cooling and diffusive escape are the main processes controlling evolution of CR electrons. Again, in the case of the Kraichnan form of the magnetic turbulence, the same ISM parameters give $\tau_{acc} \simeq 400 (E_e/\text{GeV})^{1/2} \text{Myr}$, which is still much longer than the radiative cooling timescale of electrons with $E_e > 10 \text{ GeV}$.

2.2. Transport Equation

In what follows we assume that CR electrons are injected by numerous sources throughout the ISM which has a smooth and slowly varying distribution of gas, photons, and magnetic fields relative to the relevant interaction scales discussed above. As indicated by the small mean free path calculated above, the electrons undergo multiple scattering before any

other interactions so that they acquire an isotropic pitch angle distribution. As a result, for the relevant scales of about few kpc in the vicinity of the Earth we can use the homogeneous and isotropic approximation in describing the transport of the CR electrons, where the spatial diffusion can be represented by an overall (energy dependent) escape term. Hence, ignoring turbulent acceleration, the propagation of the GeV/TeV CR electrons within the local ISM can be described by the following kinetic equation:

$$\frac{\partial n_e(E_e)}{\partial t} = -\frac{\partial}{\partial E_e} \left[\frac{E_e n_e(E_e)}{\tau_{loss}} \right] - \frac{n_e(E_e)}{\tau_{esc}} + \dot{Q}_e(E_e) \quad (2)$$

(see, e.g., Petrosian & Liu 2004, and references therein), where $\dot{Q}_e(E_e)$ denotes the injection rate of electrons, and τ_{loss} the total energy losses timescale. The steady-state solution to this equation reads as

$$n_e(E_e) = \frac{\tau_{loss}(E_e)}{E_e} \int_{E_e}^{\infty} dE'_e \dot{Q}_e(E'_e) \exp \left[- \int_{E_e}^{E'_e} \frac{dE''_e}{E''_e} \frac{\tau_{loss}(E''_e)}{\tau_{esc}(E''_e)} \right]. \quad (3)$$

For a broad, e.g. a power-law-type injection function, a very rough but illustrative approximations to this solutions are $n_e(E_e < E_0) \sim \tau_{esc} \times \dot{Q}_e$ and $n_e(E_e > E_0) \sim \tau_{loss} \times \dot{Q}_e$, where at E_0 we have $\tau_{loss}(E_0) = \tau_{esc}(E_0)$. Note that for $\tau_{loss} \simeq \tau_{rad,T}$ and τ_{esc} as specified above ($\xi \simeq 10$, and $\ell \simeq 3$ kpc, roughly the vertical scale of the Galactic disk) one has $E_0 \simeq 1$ GeV. Thus, from the precisely known transport timescales and the observed electron flux $J_e(E_e > \text{GeV}) \propto E_e^{-3}$ one can set direct constraints for the electron injection function $\dot{Q}_e(E_e)$. We note in this context that non-relativistic shock waves associated with Galactic supernova remnants (SNRs) are expected to be the primary source of the observed high-energy (> 10 GeV) CRs (e.g., Blandford & Ostriker 1978). This anticipation seems to be confirmed by the most recent X-ray and γ -ray observations regarding several remnants (see, e.g., Vink 2008, and references therein). However, the injection spectrum of CR particles (both leptons and hadrons) may be substantially different from the energy spectra of freshly accelerated electrons and ions at SNR shocks, due to a complex convolution of particle cooling, transport, and CR-driven magnetic amplification processes in vicinity of non-linear shock waves (Blandford & Eichler 1987; Caprioli et al. 2009).

In this paper we restrict the analysis to the CR electrons not affected by the solar modulation, i.e. the ones with energies $E_e > 10$ GeV, for which the escape effects can be neglected. Therefore we omit the escape term in the equation 2, and obtain

$$n_e(E_e) = \frac{\tau_{loss}(E_e)}{E_e} \int_{E_e}^{\infty} dE'_e \dot{Q}_e(E'_e), \quad (4)$$

so that for the injected function $\dot{Q}_e(E_e) \propto E_e^{-s_e}$ and $\tau_{loss} \simeq \tau_{rad,T} \propto E_e^{-1}$ the observed electron spectrum will also be a power-law, $n_e(E_e) \propto E_e^{-s_e-1}$. Hence $s_e = 2$ will be required

by the observed electron flux $J_e(E_e) \propto E_e^{-3}$. However, if the dominant electron cooling is due to the IC scattering in the KN regime, the energy losses time scale goes roughly as $\tau_{loss} \simeq \tau_{rad,KN} \propto E_e^{1/2}$, which will give rise to $n_e(E_e) \propto E_e^{-s_e+0.5}$. In other words, *within the energy range where the IC/KN losses are dominant*, the steady-state electron energy distribution is expected to pile-up above that expected from extrapolation of the Thomson-regime spectrum, as discussed in different contexts by, e.g., Aharonian & Ambartsumyan (1985); Dermer & Atoyan (2002); Kusunose & Takahara (2005); Moderski et al. (2005), and Stawarz et al. (2006). These KN-related spectral pile-ups are more and more pronounced for flatter and flatter injection continuum¹. Interestingly, as already noted in the previous section, for the characteristic energy of the starlight photons $\varepsilon_{star} \simeq 1\text{ eV}$ (wavelengths $\lambda_{star} \simeq 1\ \mu\text{m}$), this is expected to happen for $E_e \gtrsim m_e^2 c^4 / 4\varepsilon_{star} \sim 0.1\text{ TeV}$, i.e. within the range of the claimed ‘electron excess’, assuming that the energy density of the starlight emission dominates all the other Galactic photon and magnetic fields ($\xi > 1$). As a result, if the discussed KN effect plays a role, a relatively steep electron injection index $s_e > 2$ is in fact required to account for the observed spectrum $J_e(E_e) \propto E_e^{-3}$.

2.3. Energy Spectra of CR Electrons

We now present a more rigorous treatment of the KN effect and show that it may be the primary cause of the observed deviation of CR electron spectrum from a simple power law. For this purpose we need a more detailed description of the Galactic photon fields and of the radiative cooling rate. We model the Galactic dust and starlight emission by the functions $u(\varepsilon)$ similar to the ones given by Porter et al. (2006), which peak for $\varepsilon \simeq 0.015\text{ eV}$ and $\varepsilon \simeq 0.5 - 2.0\text{ eV}$ photon energies with the maximum levels u_{dust} and u_{star} , respectively, such that the total (integrated over ε) energy densities in these components are $\simeq 2 u_{dust}$ and $\simeq 3 u_{star}$. The left panels of Figure 1 show variation with photon energy of the CMB, dust and starlight energy densities for several relative values of these densities. In each panel we show three curves: for three values of u_{dust} and fixed $u_{star} = 0.3\text{ eV cm}^{-3}$ (top); three values of u_{star} and $u_{dust} = 0.3\text{ eV cm}^{-3}$ (middle); three values of $u_{dust} = u_{star}$ (bottom). We also show the energy density of the magnetic field for $B = 1\ \mu\text{G}$ (solid horizontal lines), and $3\ \mu\text{G}$ (dashed horizontal lines).

Following Moderski et al. (2005), we approximate the radiative energy loss timescale for

¹Note that the pile-up effects in the electron energy distribution resulting from the KN suppression are present at some level for any slope of the injection spectrum, unlike the analogous effects related to the synchrotron cooling alone (Kardashev 1962), which are present only for $s_e < 2$.

ultrarelativistic leptons as

$$\tau_{rad}(E_e) \simeq \frac{3m_e^2 c^3}{4\sigma_T E_e} \left[\frac{B^2}{8\pi} + \int d\varepsilon u_{tot}(\varepsilon) f_{KN}\left(\frac{4E_e \varepsilon}{m_e^2 c^4}\right) \right]^{-1}, \quad (5)$$

where the total energy density of the Galactic photon fields (including CMB radiation) is $\int d\varepsilon u_{tot}(\varepsilon)$. Here the KN correction factor is taken to be of the form

$$f_{KN}(x) \simeq \begin{cases} (1+x)^{-1.5} & \text{for } x < 10^4 \\ \frac{27}{2} x^{-2} \left(\ln x - \frac{11}{6}\right) & \text{for } x > 10^4 \end{cases}. \quad (6)$$

In addition, we consider the electron energy losses due to the Coulomb collisions and the bremsstrahlung process. The appropriate timescale of these can be approximated as, respectively,

$$\tau_{coul}(E_e) \simeq \frac{2E_e}{3 \ln \Lambda m_e c^3 \sigma_T n_{ism}}, \quad (7)$$

where $\ln \Lambda \simeq 40$ (Petrosian 1973), and

$$\tau_{brem}(E_e) \simeq \frac{2\pi}{3\alpha_{fs} \sigma_T c n_{ism} \chi(E_e)}, \quad (8)$$

where $\alpha_{fs} \simeq 1/137$ is the fine structure constant and $\chi(E_e) \simeq \ln(2E_e/m_e c^2) - 1/3 \simeq 10$ (Petrosian 2001). We note that the above form of τ_{brem} includes electron-ion and electron-electron bremsstrahlung assuming completely unscreened limit with 10% fully ionized helium abundance. With such, the total energy losses timescale is

$$\tau_{loss}^{-1}(E_e) = \tau_{coul}^{-1}(E_e) + \tau_{brem}^{-1}(E_e) + \tau_{rad}^{-1}(E_e). \quad (9)$$

The right panels of Figure 1 show the total energy losses timescales (multiplied by energy) corresponding to the photon and B field energy densities the same as in the left panels, and $n_{ism} = 1 \text{ cm}^{-3}$. As evident, at low energies $E_e \lesssim 1 \text{ GeV}$ the Coulomb and bremsstrahlung processes dominate electron cooling, since $\tau_{coul} \sim 50 (E_e/\text{GeV}) \text{ Myr}$ and $\tau_{brem} \sim 50 \text{ Myr}$ (for $n_{ism} = 1 \text{ cm}^{-3}$ and $\chi(E_e) = 10$). At higher electron energies, the IC/T losses take over. However, for $E_e > 10 \text{ GeV}$ the radiative cooling rates deviate from the ones characterizing the Thomson regime (which would be represented by horizontal lines on these plots) due to the KN effect. Note that these deviations are the strongest in the case of a large ratio u_{star}/u_{dust} . This is because for dust emission in the far-infrared range, the dominant radiative cooling is still in the Thomson regime even for relatively energetic electrons. Therefore, the KN suppression for the optical target photons becomes important only for large values of the ratio u_{star}/u_{dust} . *This is exactly the reason why the KN-related features in the CR electron spectrum discussed here may remain unnoticed in the GALPROP calculations, even*

though this code includes the exact prescription of the IC cross section, valid in both T and KN regimes.

Using this radiative loss rate in the simplified version of the kinetic equation (4) we obtain the energy flux spectrum $J_e(E_e) \propto n_e(E_e)$ of CR electrons. For the injection function $\dot{Q}_e(E_e)$ we use

$$\dot{Q}_e(E_e) = k_e E_e^{-s_e} \exp\left[-\frac{E_e}{E_{e,max}}\right], \quad (10)$$

with the normalization k_e fixed so that $[E_e^3 J_e(E_e)]_{E_e=30 \text{ GeV}} = 151.4 \text{ GeV}^2 \text{ m}^{-2} \text{ s}^{-1} \text{ sr}^{-1}$, as indicated by the Fermi data. In general, the model outlined above has seven free parameters, namely s_e , $E_{e,max}$, u_{dust} , u_{star} , B , n_{ism} , and ℓ . However, we fix for illustration $\ell = 3 \text{ kpc}$, $n_{ism} = 1 \text{ cm}^{-3}$, and $E_{e,max} = 2 \text{ TeV}$, so that we are left with only four free parameters s_e , u_{dust} , u_{star} , and B . We note in this context that the direct measurements of the Galactic photon and magnetic field energy densities are difficult due to substantial foregrounds, and thus the associated uncertainties are relatively large (e.g., Crutcher et al. 2003; Hauser & Dwek 2001). Below we explore the corresponding parameter space of the model.

Figure 2 shows the energy spectra of primary electrons corresponding to two different injection spectral indices, $s_e = 2.0$ and 2.2 , and to the same choice of the values of the other three model parameters used in Figure 1. As evident, the expected KN pile-up effects are indeed present, being the most pronounced for flatter injection continuum, and for large values of the ratio u_{star}/u_{dust} . The value for the ISM magnetic field have little effect on the results, as long as $B < 10 \mu\text{G}$. One conclusion here is that different combinations of the parameters s_e , u_{star} , and u_{dust} can lead to the observed electron spectrum $J_e(E_e) \propto E_e^{-3}$. However, our primary result is that it is relatively easy to account for a possible minor excess in the energy distribution of primary CR electrons over this power law in the $0.1 - 1 \text{ TeV}$ energy range purely by the KN effect.

In Figure 3 we compare the observed spectra from various experiments with one of our model calculations corresponding to a choice of model parameters appropriate for the average (local) ISM conditions, namely $\ell = 3 \text{ kpc}$, $n_{ism} = 1 \text{ cm}^{-3}$, $B = 3 \mu\text{G}$, $u_{dust} = 0.1 \text{ eV cm}^{-3}$, $u_{star} = 3 \text{ eV cm}^{-3}$, $E_{e,max} = 2.75 \text{ TeV}$, and $s_e = 2.42$. The data points correspond to different measurements by ATIC (black; Chang et al. 2008), PPB-BETS (yellow; Torii et al. 2008), emulsion chambers (magenta; Kobayashi et al. 2004), HESS (blue and cyan; Aharonian et al. 2008, 2009a, respectively), and Fermi (red; Abdo et al. 2009). As evident, with reasonable parameters² and the electron injection index the same as required for the Galactic CR protons,

²It is important to note in this context that the anticipated value of the starlight energy density, $u_{star} = 3 \text{ eV cm}^{-3}$, even though considered here as a ‘reasonable’ one, is still larger than that expected for the local

$s_e = s_p = 2.42$ (see section 3.1 below), we can reproduce very well the latest, and most reliable observations by Fermi and HESS. It is also clear that the KN effect cannot account for the sharp feature claimed by ATIC observations. Encouraged by this simple and robust explanation for the primary CR electron spectrum, in the next section we also explore the influence of the KN effect on the expected spectra of secondary e^\pm pairs with the goal of providing explanation of the rise with energy of the positron to electron ratio observed by PAMELA.

3. Secondary and Tertiary Pairs

In this section we address the question of the origin and spectrum of ultrarelativistic positrons present in the CR population, which are produced as secondaries in e^\pm pair production processes. We consider three different sources of secondary e^\pm pairs and apply the same transport equation as above to determine their spectra in the ISM. From these we obtain the positron to electron ratio and compare it to the observation by PAMELA.

3.1. Proton-Proton Pair Production

The first source of secondary pairs we consider is due to the interactions of ultrarelativistic CR ions (primarily protons) with the ambient plasma. We assume that the Galactic sources of CRs in addition to electrons inject also ultrarelativistic protons at a constant rate $\dot{Q}_p(E_p) \propto E_p^{-s_p}$, which then propagate diffusively through the ISM and collide with cold protons. The appropriate timescale for the proton-proton interaction is roughly independent of energy: $\tau_{pp} \simeq (c n_{ism} \sigma_{pp})^{-1} \simeq 30 (n_{ism}/\text{cm}^{-3})^{-1} \text{Myr}$ for the cross-section $\sigma_{pp} \simeq 3.4 \times 10^{-26} \text{cm}^2$ (see, e.g., Kelner et al. 2006). The diffusive escape timescale for CR protons is same as for electrons, namely $\tau_{esc} \simeq 100 (E_p/\text{GeV})^{-1/3} \text{Myr}$ (for $\ell \simeq 3 \text{kpc}$, and $n_{ism} \simeq 1 \text{cm}^{-3}$). This means that CR protons with $E_p > 30 \text{GeV}$ are in a slow cooling regime (i.e., we are dealing with a thin target case), so that the ISM proton energy spectrum can be approximated as $n_p(E_p > 30 \text{GeV}) \simeq \tau_{esc} \times \dot{Q}_p(E_p) \propto E_p^{-s_p-1/3}$ (for the Kolmogorov turbulence; see the discussion in section 2.1 and below equation 3). Keeping in mind the observed CR proton flux $J_p(E_p) \propto E_p^{-2.75}$, the required injection spectral index should be then $s_p \simeq 2.42$. In addition, in this regime protons escape with most of their

ISM (Strong et al. 2000; Porter et al. 2006; Moskalenko et al. 2006; Porter et al. 2008). As such, it should be considered as an illustrative model assumption, for which the analyzed KN effects are already of a major importance (see the related discussion in §3.4 and §4 further below).

energy and only a small fraction f of the carried flux goes into production of secondaries (e^\pm and neutrinos arising from π^\pm decays) and γ -rays (from π^0 decay). In particular, one has $f \simeq \tau_{esc}/\tau_{pp} \simeq 0.3 (E_p/\text{TeV})^{-1/3}$. Note that if the CR protons propagate through the ISM with some particular bulk velocity, e.g., of the order of the Alfvén speed, the situation may change. For example, with $\tau_{dyn} \simeq \ell/v_A$ one gets $f \simeq \tau_{dyn}/\tau_{pp} \simeq 10$ independent of the proton energy (for $B \simeq 3 \mu\text{G}$, $\ell \simeq 3 \text{kpc}$, and $n_{ism} \simeq 1 \text{cm}^{-3}$). In this case one would expect $n_p(E_p) \simeq \tau_{pp} \times \dot{Q}_p(E_p) \propto E_p^{-s_p}$, requiring thus a steeper injection index of $s_p \simeq 2.75$.

Independent of which CR proton propagation model is the correct one, the production rate of the secondary pairs will depend on the observed spectrum of the CR protons (which we assume to be the same throughout the Galactic disk):

$$\dot{Q}_{e^\pm}(E_{e^\pm}) \simeq \tau_{pp}^{-1} n_p(E_p) f_{e^\pm}(E_{e^\pm}/E_p), \quad (11)$$

where $f_{e^\pm}(E_{e^\pm}/E_p)$ is the number of pairs with energy E_{e^\pm} produced by a CR proton of energy E_p . Detailed calculations by Kelner et al. (2006) show that for $1 \text{TeV} \lesssim E_p \lesssim 1 \text{PeV}$, the function $f_{e^\pm}(E_{e^\pm}/E_p)$ is strongly peaked for $E_{e^\pm}/E_p \simeq 0.07$ at the level $f_{e^\pm}^{max} \simeq f_{e^\pm}(0.07) \simeq 4$. As a result, the injection function of the secondary pairs should follow the energy spectrum of CR protons, namely $\dot{Q}_{e^\pm}(E_{e^\pm}) \propto E_{e^\pm}^{-s_p}$. Since the secondary pairs obey the same transport equation as the primary electrons, their spectra can be calculated as discussed in §2. In particular, for high energies the escape term (as well as the Coulomb and bremsstrahlung energy losses) can be ignored giving $n_{e^\pm}(E_{e^\pm} > 10 \text{GeV}) \simeq \tau_{rad} \times \dot{Q}_{e^\pm}(E_{e^\pm}) \propto E_{e^\pm}^{-s_p-1}$ for $\tau_{rad} \simeq \tau_{rad,T}$. More generally, the expected secondary pair to total electron ratio should vary with the energy roughly as

$$\begin{aligned} \left. \frac{n_{e^\pm}}{n_e} \right|_{pp} &\simeq \frac{\tau_{rad}(E_e)}{\tau_{pp}} \frac{4 J_p(14E_e)}{J_e(E_e)} \\ &\xrightarrow{T} 4 \left(\frac{n_{ism}}{\text{cm}^{-3}} \right) \left(\frac{u_{star}}{\text{eV cm}^{-3}} \right)^{-1} \left(\frac{E_e}{\text{GeV}} \right)^{-0.75}, \end{aligned} \quad (12)$$

where $J_p(E_p) \simeq 2.2 \times 10^4 (E_p/\text{GeV})^{-2.75} \text{GeV}^{-1} \text{m}^{-2} \text{s}^{-1} \text{sr}^{-1}$ is the observed CR proton flux, and $J_e(E_e) \simeq 155 (E_e/\text{GeV})^{-3} \text{GeV}^{-1} \text{m}^{-2} \text{s}^{-1} \text{sr}^{-1}$ is the observed CR electron flux. The last line in the above equation assumes we are in the Thomson regime with $\tau_{rad} \simeq \tau_{rad,T} \propto E_{e^\pm}^{-1}$ so that this ratio becomes $n_{e^\pm}/n_e \propto E_e^{-0.75}$ with the particular value $(n_{e^\pm}/n_e)_{100 \text{GeV}} \simeq 0.04$ for the assumed starlight density of $u_{star} \simeq 3 \text{eV cm}^{-3}$. This is in a disagreement with the PAMELA results indicating the e^\pm fraction increasing with energy up to $(n_{e^\pm}/n_e)_{100 \text{GeV}} > 0.1$ (Adriani et al. 2009). However, as discussed above, at higher energies we are in the KN regime, where $\tau_{rad} \simeq \tau_{rad,KN} \propto E_e^{1/2}$, which will give rise to a flatter energy spectrum of the secondary pairs and hence to $n_{e^\pm}/n_e \propto E_e^{0.75}$. Note also that, since $\tau_{rad,T} \propto u_{star}^{-1}$, in regions of low (high) radiative field densities the expected e^\pm fraction will be higher (lower) for a given $J_p(E_p)$ and $J_e(E_e)$.

3.2. Photo-Pair Production

One possibility for increasing the pair fraction in the CR spectrum is to introduce an additional, flatter spectral component consisting solely of the e^\pm pairs that outnumber the secondaries resulting from the proton-proton interactions³. However, this population cannot extend up to $E_e > 1$ TeV energies, since this would violate the high-energy cut-off measured in the CR electron spectrum by the HESS experiment (Aharonian et al. 2008). A possible source of pairs that satisfy these requirements may be due to photon-photon annihilation of TeV-energy γ -rays on starlight (Aharonian & Atoyan 1991; Mastichiadis et al. 1991). The cross-section for this process has a sharp peak when photon energies satisfy the condition $\varepsilon_0 \varepsilon_\gamma = 2m_e^2 c^4$. Thus, the annihilation of $\varepsilon_0 \simeq \varepsilon_{star} \simeq 1$ eV and $\varepsilon_\gamma \simeq 0.5$ TeV γ -ray photons will inject into the ISM a relatively narrow energy distribution of pairs at the rate $\dot{Q}_{e^\pm, \gamma\gamma}(E_{e^\pm}) \propto \delta(E_{e^\pm} - m_e^2 c^4 / \varepsilon_{star})$. Such a distribution cooling radiatively according to equation (4) will produce a flat-spectrum $n_{e^\pm}(E_{e^\pm}) \propto E_{e^\pm}^{-2}$ (in the Thomson regime, or even a flatter one in the KN regime), instead of $\propto E_{e^\pm}^{-3.75}$ expected for the secondaries resulting from the decay of π^\pm generated in the proton-proton interactions, as described above.

However, the question is whether there will be sufficient number of such pairs to account for the PAMELA observations. In order to address this issue we use the δ -function approximation for the photon-photon annihilation cross section $\sigma_{\gamma\gamma}(\varepsilon_0, \varepsilon_\gamma) \simeq (1/3) \sigma_T \varepsilon_0 \delta[\varepsilon_0 - (2m_e^2 c^4 / \varepsilon_\gamma)]$ (Zdziarski & Lightman 1985), from which we can calculate the absorption coefficient $\alpha_{\gamma\gamma}(\varepsilon_\gamma) = \int_{m_e c^2 / \varepsilon_0} d\varepsilon_0 n_0(\varepsilon_0) \sigma_{\gamma\gamma}$. If we also approximate the energy density of the soft (starlight) photon field by a monoenergetic distribution with total density n_{star} and energy ε_{star} , namely $n_0(\varepsilon_0) = n_{star} \delta(\varepsilon_0 - \varepsilon_{star})$ such that $\int d\varepsilon_0 u_0(\varepsilon_0) = u_{star} = n_{star} \varepsilon_{star}$, then the opacity becomes $\alpha_{\gamma\gamma}(\varepsilon_\gamma) \simeq (\sigma_T / 3) u_{star} \delta[\varepsilon_{star} - (2m_e^2 c^4 / \varepsilon_\gamma)]$. From this we can evaluate the optical depth to be

$$\tau_{\gamma\gamma}(\varepsilon_\gamma) \simeq \tau_{\gamma\gamma}^0 \times \delta\left[\varepsilon_{star} - \frac{2m_e^2 c^4}{\varepsilon_\gamma}\right], \quad (13)$$

where

$$\tau_{\gamma\gamma}^0 \equiv \frac{1}{3} \ell \sigma_T u_{star} \varepsilon_{star}^{-1} \simeq 2 \times 10^{-3} \left(\frac{\ell}{3 \text{ kpc}}\right) \left(\frac{u_{star}}{\text{eV cm}^{-3}}\right) \left(\frac{\varepsilon_{star}}{\text{eV}}\right)^{-1}. \quad (14)$$

Since $\tau_{\gamma\gamma}^0 \ll 1$, most of the γ -rays freely escape the Galaxy and thus their number density per energy is $n_\gamma(\varepsilon_\gamma) \simeq (\ell/c) \dot{Q}_\gamma(\varepsilon_\gamma)$, where $\dot{Q}_\gamma(\varepsilon_\gamma)$ is the γ -ray production rate discussed below.

³Note that such a population cannot be accompanied by the additional population of proton-antiproton pairs, since this would violate the observed proton-to-antiproton ratio (Moskalenko et al. 2002).

3.2.1. Tertiary Pairs from Hadronic Interactions

Proton-proton interactions, in addition to producing secondary pairs, also produce γ -rays (from π^0 decay) of similar spectrum and comparable intensity. These γ -rays could be the source of the e^\pm pairs (which may be called tertiary pairs) in the above scenario. The rate of such ‘hadronic’ γ -ray production may be approximated as

$$\dot{Q}_{\gamma,pp}(\varepsilon_\gamma) \simeq \tau_{pp}^{-1} n_p(E_p) f_\gamma(\varepsilon_\gamma/E_p), \quad (15)$$

where $f_\gamma(\varepsilon_\gamma/E_p)$ is the number of photons with energy ε_γ produced in a single proton-proton collision involving a CR proton with the energy E_p . Just as in the case of secondary pair production, we refer to Kelner et al. (2006), who showed that in the range $0.1 \text{ TeV} \lesssim E_p \lesssim 1 \text{ PeV}$ the function $f_\gamma(\varepsilon_\gamma/E_p)$ is peaked for $\varepsilon_\gamma/E_p \simeq 0.1$ at the level $f_\gamma^{max} \simeq f_\gamma(0.1) \simeq 6$.

The total production rate of such tertiary e^\pm pairs (with energies $E_e \simeq \varepsilon_\gamma/2$) may be obtained from $\dot{Q}_{e^\pm,\gamma\gamma}(E_e) \simeq 4c \alpha_{\gamma\gamma} n_\gamma(\varepsilon_\gamma)|_{\varepsilon_\gamma=2E_e}$ (Coppi & Blandford 1990). As before, inserting this in equation (4) and carrying out the integration, we get the density ratio of tertiary pairs to total electrons at the same energy E_e in terms of the observed CR proton and electron flux ratio,

$$\begin{aligned} \left. \frac{n_{e^\pm}}{n_e} \right|_{\gamma\gamma/pp} &\simeq 24 \tau_{\gamma\gamma}^0 \frac{\tau_{rad}(E_e)}{\tau_{pp}} \frac{m_e^2 c^4}{E_e \varepsilon_{star}} \frac{J_p(20m_e^2 c^4/\varepsilon_{star})}{J_e(E_e)} \\ &\xrightarrow{\text{T}} 10^{-6} \left(\frac{\ell}{3 \text{ kpc}} \right) \left(\frac{n_{ism}}{\text{cm}^{-3}} \right) \left(\frac{\varepsilon_{star}}{\text{eV}} \right)^{0.75} \left(\frac{E_e}{\text{GeV}} \right), \end{aligned} \quad (16)$$

where for the the bottom line we have assumed $u_{star} \simeq u_{tot}$ and used the Thomson regime for $\tau_{rad}(E_e)$.

First, we note that because $\tau_{\gamma\gamma}^0 \ll 1$ (see equation 13) the expected number of (tertiary) pairs from photo-pair process will be lower than that of the (secondary) pairs from proton-proton interaction. Second, because $\tau_{\gamma\gamma}^0 \propto u_{star}$ and in the Thomson regime $\tau_{rad} \propto u_{star}^{-1}$, the ratio of photo-pairs to primary electron is independent of the energy density of the soft photon field, as long as it dominates over the other Galactic photon fields and the magnetic field. However, more importantly, this ratio increases with increasing starlight energy as $n_{e^\pm}/n_e \propto \varepsilon_{star}^{0.75}$, and (in the Thomson regime) it increases linearly with electron energy. Therefore, in regions of the Galaxy containing high energy (ultraviolet) photons and for high energy electrons the photo-pair production may become important and even dominant (see below). Of course, the above result again will be modified by the inevitable KN effect. In this context it should be emphasized that because of the flatter injection function of the tertiary pairs resulting from the photon-photon annihilation the KN effect should be more pronounced for them than for the primary electrons or the secondary pairs originating from the decay of π^\pm due to proton-proton collisions.

3.2.2. Tertiary Pairs from Leptonic Interactions

Yet another source of γ -rays which may annihilate on the starlight photon field and create additional e^\pm population is provided by the IC emission of CR electrons themselves. In order to estimate the expected relevance of this process, we need the rate of production of γ -rays, $\dot{Q}_{\gamma,ic}(\varepsilon_\gamma)$, which will take the place of $\dot{Q}_{\gamma,pp}(\varepsilon_\gamma)$ specified in the previous section. The IC rate is related to the IC emissivity $j_{ic}(\varepsilon_\gamma)$ as $\dot{Q}_{\gamma,ic}(\varepsilon_\gamma) = 4\pi j_{ic}(\varepsilon_\gamma)/\varepsilon_\gamma$, which can be obtained from the standard relation $[\varepsilon_\gamma j_{ic}(\varepsilon_\gamma)] \simeq (1/4\pi) [E_{e,ic}^2 n_e(E_{e,ic})]/\tau_{rad}(E_{e,ic})$. Here $E_{e,ic}$ is the energy of electrons emitting γ -ray photons with energies ε_γ , while $\tau_{rad}(E_{e,ic})$ includes only IC cooling due to soft photons of energy ε_{star} . This gives

$$\dot{Q}_{\gamma,ic}(\varepsilon_\gamma) = \left(\frac{E_{e,ic}}{\varepsilon_\gamma} \right)^2 \frac{n_e(E_{e,ic})}{\tau_{rad}(E_{e,ic})}, \quad (17)$$

which replaces the photon production rate given above in equation (15).

Following the same procedure as above we can evaluate the density of γ -rays, the rate of production of e^\pm pairs $\dot{Q}_{e^\pm,\gamma\gamma}(E_{e^\pm})$, and then the density of pairs in the ISM. In the Thomson regime $\varepsilon_\gamma \simeq (4/3) E_{e,ic}^2 \varepsilon_{star}/m_e^2 c^4$ and thus $(E_{e,ic}/\varepsilon_\gamma)^2 = 3/8$ for $\varepsilon_{star} = 2m_e^2 c^4/\varepsilon_\gamma$, while in the KN regime $E_{e,ic}/\varepsilon_\gamma \simeq 1$. As we will see below, for relevant CR energies we are closer to the KN regime so we will ignore the factor 3/8. We then obtain

$$\begin{aligned} \left. \frac{n_{e^\pm}}{n_e} \right|_{\gamma\gamma/ic} &\simeq 4 \tau_{\gamma\gamma}^0 \frac{m_e^2 c^4}{E_e \varepsilon_{star}} \frac{[J_e(E_e)/\tau_{rad}]_{E_e=2m_e^2 c^4/\varepsilon_{star}}}{[J_e(E_e)/\tau_{rad}]} \\ &\xrightarrow{\text{T}} 8 \times 10^{-6} \left(\frac{\ell}{3 \text{ kpc}} \right) \left(\frac{u_{star}}{\text{eV cm}^{-3}} \right) \left(\frac{E_e}{\text{GeV}} \right) \end{aligned} \quad (18)$$

where the last line is evaluated for the Thomson regime with $\tau_{rad} \propto E_e^{-1}$. As evident, in this regime and for the observed $J_e(E_e)$ we obtain $(n_{e^\pm}/n_e)_{100 \text{ GeV}} \simeq 2 \times 10^{-3}$ for $\ell \simeq 3 \text{ kpc}$ and $u_{star} \simeq 3 \text{ eV cm}^{-3}$, independent of the soft photon energy. This implies that the production of TeV-energy γ -rays via IC emission of CR electrons — if proceeding in the Thomson regime — may dominate over the one resulting from the protons-proton interactions. On the other hand, the KN effect are expected to reduce the IC emissivity of ultrarelativistic e^\pm pairs within the consider photon energy range, and therefore both hadronic and leptonic processes may be in fact comparable. For the choice of model parameters appropriate for the average ISM conditions, this is not enough to account for the high positron fraction found in the CR spectrum.

3.3. Energy Spectra of Secondaries and Tertiaries

As in case of primary electrons we now carry a more accurate determination of secondary and tertiary pairs by omitting most of the approximations used above. The production rate of the secondary pairs from proton-proton interactions is now obtained from

$$\dot{Q}_{pp}(E_e) = \frac{1}{\tau_{pp}} \int_{E_e} \frac{dE_p}{E_p} J_p(E_p) f_e(E_p, E_e), \quad (19)$$

where we use the analytic approximation for the function $f_e(E_p, E_e)$ as given in Kelner et al. (2006), and fix $J_p(E_p) \simeq 2.2 \times 10^4 (E_p/\text{GeV})^{-2.75} \text{ GeV}^{-1} \text{ m}^{-2} \text{ s}^{-1} \text{ sr}^{-1}$. For the production rates of (tertiary) pairs generated from annihilation of high-energy γ -rays with density $n_\gamma(\varepsilon_\gamma)$ by the soft Galactic photon fields, we write analogously

$$\dot{Q}_{\gamma\gamma}(E_{e^\pm}) = \frac{4}{3} \sigma_T c u_{\text{rad}}(\varepsilon)|_{\varepsilon=m_e^2 c^4/E_{e^\pm}} n_\gamma(\varepsilon_\gamma)|_{\varepsilon_\gamma=2E_{e^\pm}}, \quad (20)$$

where again we have used the delta function approximation for the photon-photon annihilation cross section as before. For the expected small optical depth of photon-photon annihilation ($\tau_{\gamma\gamma}^0 \ll 1$, see above), the spectrum of γ -rays resulting from the proton-proton interactions is given by

$$n_{\gamma/pp}(\varepsilon_\gamma) = \frac{\ell}{c \tau_{pp}} \int_{\varepsilon_\gamma} \frac{dE_p}{E_p} J_p(E_p) f_\gamma(E_p, \varepsilon_\gamma), \quad (21)$$

with the function $f_\gamma(E_p, \varepsilon_\gamma)$ denoting the number of photons with energy ε_γ produced in a single collision involving ultrarelativistic proton with energy E_p . Again, here we take the analytical approximation for $f_\gamma(E_p, \varepsilon_\gamma)$ as given in Kelner et al. (2006), noting that for $E_p \simeq 0.1 \text{ TeV} - 1 \text{ PeV}$ this may be further approximated by a simple function

$$f_\gamma(x) \simeq 2.5 x^{-1} \exp[-9 x^{0.83}], \quad (22)$$

with $x \equiv \varepsilon_\gamma/E_p$ (see in this context Hillas 2005).

Finally, for the case of γ -rays resulting from the IC emission of ultrarelativistic CR leptons, we calculate the appropriate photon energy spectrum as

$$n_{\gamma/ic}(\varepsilon_\gamma) = \frac{4\pi\ell}{c\varepsilon_\gamma} j_{ic}(\varepsilon_\gamma), \quad (23)$$

where the IC emissivity $j_{ic}(\varepsilon_\gamma)$ is related to the observed electron flux using the standard IC formulae with the KN effect included (Blumenthal & Gould 1970). We fix this flux as $J_e(E_e) \simeq 155 (E_e/\text{GeV})^{-3} \text{ GeV}^{-1} \text{ m}^{-2} \text{ s}^{-1} \text{ sr}^{-1}$ (and cutting-off exponentially at $E_e = 2 \text{ TeV}$). Inserting then the resulting e^\pm pair production rates in equation (4), we obtain the individual

and total e^\pm pair fluxes $J_{e^\pm}^{tot}(E_e) = J_{e^\pm}^{pp}(E_e) + J_{e^\pm}^{\gamma\gamma/pp}(E_e) + J_{e^\pm}^{\gamma\gamma/ic}(E_e)$ for all three mechanisms discussed above and for the same seven parameters s_e , $E_{e,max}$, u_{dust} , u_{star} , n_{ism} , ℓ and B used in calculation of the primary electron spectra.

Figure 4 shows the energy spectra of secondary leptons produced in proton-proton collisions, $J_{e^\pm}^{pp}(E_e)$ (solid lines), and of tertiary pairs produced via absorption of high-energy γ -rays generated in either hadronic or leptonic processes (dashed and dotted lines, respectively), $J_{e^\pm}^{\gamma\gamma/pp}(E_e)$ and $J_{e^\pm}^{\gamma\gamma/ic}(E_e)$, for the same set of parameters used in Figure 1 with same colors, except for the magnetic field set at $B = 1 \mu\text{G}$. As shown, the cases with a weak starlight but strong dust emission are quantitatively similar to the cases when the dust and starlight energy densities are comparable. Only in the cases when the ratio u_{star}/u_{dust} is high, the KN effect flattens the energy distribution of secondary leptons resulting from proton-proton interactions significantly, and only at high ($E_e > 100 \text{ GeV}$) energies. In all the above cases, however, the direct e^\pm pair production in the proton-proton collisions is the dominant source of the positrons, and the contribution of the other two processes (i.e., of the tertiary pairs) to the positron flux is less than 1% except at high energies where it could reach 10%. The contribution of secondary and tertiary electrons to the observed electron spectrum is even less, being on the order of $< 10\%$ and $\lesssim 0.1\%$ for proton-proton and photo-pair processes, respectively.

The above result is illustrated in Figure 5, where we compare with different measurements the computed ratio of (both secondary and tertiary) positron and electron fluxes, normally denoted in the literature as $\phi(e^+)$ and $\phi(e^-)$, respectively,

$$\frac{\phi(e^+)}{\phi(e^+) + \phi(e^-)} \equiv \frac{1}{2 [J_e(E_e)/J_{e^\pm}^{tot}(E_e)] + 1} \quad (24)$$

for the same model parameters as considered in Figure 3 (namely $u_{star} = 3 \text{ eV cm}^{-3}$, $n_{ism} = 1 \text{ cm}^{-3}$, $u_{dust} = 0.1 \text{ eV cm}^{-3}$, $B = 3 \mu\text{G}$, $\ell = 3 \text{ kpc}$, $s_e = 2.42$ and $E_{e,max} = 2.75 \text{ TeV}$). Here red symbols denote the PAMELA data (Adriani et al. 2009), cyan and blue symbols the HEAT data (Barwick et al. 1997; Beatty et al. 2004), yellow symbols the CAPRICE data (Boezio et al. 2000), and the magenta ones the measurements with the imaging calorimeter (Golden et al. 1994). As evident, due to the KN effects and inclusion of tertiary pairs the e^\pm fraction decreases only by a factor of 2 between $E_e \simeq 10 \text{ GeV}$ and 200 GeV . Even though this is a much less rapid decrease than typically expected (see Moskalenko & Strong 1998), the PAMELA results in the high energy ($E_e > 20 \text{ GeV}$) range cannot be reproduced with our conservative choice of model parameters.

3.4. High Positron Fraction

The above results show that it would be rather difficult to increase the fraction of secondary e^\pm pairs just by the photo-pair processes for the average ISM conditions. One needs different conditions for the production of the relatively high positron-to-electron fraction in the CR spectrum which also increases with energy, as claimed by the PAMELA experiment. In our model, those would require increasing the energy density of the starlight emission up to $u_{star} \sim 300 \text{ eV cm}^{-3}$, and of the ISM number density up to $n_{ism} \sim 80 \text{ cm}^{-3}$, keeping at the same time relatively low level of dust emission ($u_{dust} \sim 0.1 \text{ eV cm}^{-3}$) and magnetic field strength ($B \leq 10 \mu\text{G}$). Figure 6 (bottom panel) shows the e^\pm fraction expected for such a choice of model parameters, which agrees with the PAMELA data within the energy range not affected by the solar modulation. The corresponding total electron spectrum is compared with the Fermi and HESS data in the top panel of Figure 6. As evident we get again a very good agreement but now we need an even steeper injection spectrum of the primary electrons ($s_e \simeq 2.65$).

The set of model parameters considered in Figure 6 should be regarded as illustrative one only, not necessarily being justified for the local ISM. We note, however, that it corresponds to the optical depth for annihilation of Galactic γ -rays formally less than (though close to) unity (see equation 14), and to a small (< 0.1) ratio of number densities of γ -ray photons and CR electrons with the same energy ε , as required. In fact, we have

$$\frac{n_\gamma(\varepsilon)}{n_e(\varepsilon)} \simeq \frac{n_{\gamma,pp}(\varepsilon)}{n_e(\varepsilon)} \simeq \frac{6 \ell}{c \tau_{pp}} \frac{J_p(10 \varepsilon)}{J_e(\varepsilon)} \sim 5 \times 10^{-4} \left(\frac{n_{ism}}{\text{cm}^{-3}} \right) \left(\frac{\varepsilon}{\text{GeV}} \right)^{0.25} \quad (25)$$

(see the discussion in section 3.2 above).

The invoked increased level of the starlight energy density and of the gas number density could be more appropriate around supernova remnants where the injection of the Galactic CRs is taking place. Hence, the results of our analysis may indicate that ultrarelativistic particles generated in the Galaxy undergo most of their interactions near their sources, but propagate much more freely from these regions to the Earth (see in this context recent discussion in Higdon et al. 2009; Cowsik & Burch 2009). In fact it may be sufficient if high-energy positrons, but not necessarily electrons, are trapped in the regions characterized by the enhanced photon and gas densities. There may be even physical justification for such a situation. For example, CR protons streaming along large-scale magnetic field in the far upstream of supernova shocks with super-Alfvénic speed may excite resonant Alfvén waves in a form of coherent circularly-polarized cyclotron radiation (Lerche 1967; Kulsrud & Pearce 1969; Cesarsky 1980). Due to the particular helicity of the generated waves, they will interact with positrons of gyroradii comparable to their wavelenghts (i.e., to gyroradii of CR protons generating the turbulence), but not with the electrons. As a result, the electrons

will propagate much more freely along the Galactic magnetic field to the Earth, experiencing the ‘average’ ISM conditions⁴. The results presented in Figure 3 regarding the observed CR electron spectrum would then be appropriate. CR positrons, on the other hand, will undergo enhanced scattering in vicinities of their sources resulting in their increased fraction in the observed CR spectrum around 100 GeV energies, as presented in Figure 6 (bottom panel). A quantitative description of such a possibility would require different treatment of the positron and electron transport within the Galaxy. This is beyond the scope of this paper. The point is, however, that the efficient trapping of TeV-energy CRs in vicinities of supernova remnants, either charge-dependent or not, may justify the high values for the starlight and gas densities invoked to explain the PAMELA data in a framework of our model.

Let us mention in this context that in the local environments of SNRs additional processes may operate leading to an increase in the CR positron-to-electron fraction. These include enhanced interactions of freshly accelerated CR protons with an intense high-energy photon field of young remnants, generating thus additional secondary e^\pm pairs via the photo-meson production process (Hu et al. 2009), or the direct acceleration of secondary pairs injected into the immediacy of SNR shocks via pp collisions (Blasi 2009).

Yet one more process which may be relevant in the discussed context is the creation of e^\pm pairs by photons in the electromagnetic field of ultrarelativistic electrons, referred in the literature as a ‘triplet pair production’ (TPP; see Mastichiadis et al. 1986; Mastichiadis 1991; Dermer & Schlickeiser 1991). This process occurs when the energy of the incident photon in the electron rest frame exceeds 4 times the rest energy of the electron, $\varepsilon' > \varepsilon_{cr} \equiv 4m_e c^2$. For the starlight parameters considered in this paper, namely $\varepsilon \simeq 1$ eV, this criterium is marginally fulfilled only in the ‘head-on’ interactions with the highest energy electrons, $E_e \simeq 1$ TeV, since only in such a case $\varepsilon' \simeq 2\varepsilon E_e/m_e c^2 \sim 2\varepsilon_{cr}$. For all the other angles between the direction of an interacting electron and starlight photon, and for all the lower-energy electrons, we have obviously $\varepsilon' \ll \varepsilon_{cr}$. Nevertheless, the TPP may be of a primary importance if the soft photon energies are higher than anticipated here, say $\varepsilon \simeq 10$ eV. Then the head-on collisions of such UV photons with the TeV-energy electrons will produce effectively e^\pm pairs with energies $E_{e^\pm} \sim 0.5 (E_e/\varepsilon)^{1/2} m_e c^2 \sim 0.1$ TeV (see Dermer & Schlickeiser 1991), i.e. exactly within the energy range of the PAMELA excess. Note that the energy losses of thus produced pairs should be dominated by the IC scattering deep in the KN regime, and hence the spectral pile-ups discussed in this paper will flatten additionally the injected positron spectrum around $E_e \sim 10 - 100$ GeV energies. That is because the TPP cross-section, $\sigma_{TPP} \sim \alpha_{fs} \times \sigma_T$, exceeds the IC cross section (due to the KN suppression of the

⁴Note that the returning current will be assured by the ambient plasma, and would involve sub-thermal bulk velocities of ISM particles due to the expected high number density of ISM within the Galactic disk.

latter one) only for $\varepsilon' > 300 m_e c^2$, while the TPP cooling rate exceeds the IC cooling rate only for $\varepsilon' > 10^5 m_e c^3$ (Mastichiadis 1991; Dermer & Schlickeiser 1991). As a result, if the sources of Galactic CRs are associated with an intense UV photon field, the most recent PAMELA results may be possibly explained with much less extreme ISM parameters than discussed in this section.

4. Summary and Discussion

In this paper we show that the observed excesses in the energy distribution of the Galactic CR electrons around energies $E_e \sim 0.1 - 1$ TeV may be easily re-produced without invoking any unusual source of ultrarelativistic electrons (or e^\pm pairs), such as dark matter annihilation/decay or some nearby astrophysical object (e.g. a pulsar), other than the general diffuse Galactic components of CR electrons and protons injected by supernova remnants. The model presented here assumes an injected spectrum of electrons (power-law with index s_e) and evaluates their observed energy distribution based on a simple and most commonly invoked kinetic equation describing the propagation of CR electrons in the ISM. The main process affecting this outcome is the cooling of the injected electrons by their interaction with the ISM photons (via IC scattering). The interactions of electrons with ISM turbulence produces negligible re-acceleration and determines their escape time. The escape timescale also turns out to be somewhat longer than the cooling time in the relevant range of electron energies. The new physical effect that is the source of the observed excess is the Klein-Nishina suppression of the IC cooling rate, which becomes important right around TeV energies. With a very reasonable choice of the model parameters characterizing the local interstellar medium ($u_{star} \sim 3 \text{ eV cm}^{-3}$, $u_{dust} \sim u_{cmb} \sim 0.3 \text{ eV cm}^{-3}$, $B \sim 3 \mu\text{G}$, and $n_{ism} \sim 1 \text{ cm}^{-3}$) we can reproduce the most recent, and perhaps the most reliable observations by Fermi and HESS, but not the sharp feature claimed by ATIC. Interestingly, in our model the injection spectral index of CR electrons becomes comparable to, or perhaps equal to that of CR protons, namely $s_e \simeq s_p \simeq 2.4$.

The Klein-Nishina effect will also affect the propagation of the secondary e^\pm pairs and can produce deviations from a power-law in the observed spectra of such pairs. In particular, it can affect the positron-to-electron ratio. We have explored this possibility by considering two mechanisms for production of e^\pm pairs (and therefore positrons). The first is production of pairs due to the decay of π^\pm 's generated by interaction of CR nuclei with ambient protons. The second source discussed here is the pair production due to annihilation of diffuse Galactic γ -rays interacting with the starlight photon field. We consider two sources of the Galactic γ -rays. The first is related to the decay of π^0 's also produced in proton-proton interactions

and the second is due to the IC scattering of primary CR electrons by the diffuse Galactic photon fields. We show that indeed there will be deviations from a simple power-law in the spectra of thus created e^\pm pairs (as well as in the positron-to-electron flux ratio), similar to the observed one. However, the relatively high observed positron fraction that increases quite steeply with energy, as observed by PAMELA, cannot be explained by the conservative set of the model parameters used above, which corresponds to the average values expected in the Galactic disk. We can however reproduce the PAMELA result by increasing the energy density of the starlight photon field and of the ISM number density up to the levels $u_{star} \sim 300 \text{ eV cm}^{-3}$ and $n_{ism} \sim 80 \text{ cm}^{-3}$. With these new values we can also fit the Fermi and HESS data, though with somewhat steeper injected spectrum of the primary electrons than required before ($s_e \sim 2.65$).

The required increased level of the starlight energy density and of the gas number density may be regarded as unlikely for the local interstellar medium. However, such a choice of the model parameters could be more appropriate around supernova remnants where the injection of the Galactic CRs is taking place. A possible solution to this problem may be that CRs undergo most of their interactions near their sources, being efficiently trapped thereby by self-generated CR-driven turbulence. Interestingly, such a trapping may be charge-dependent, affecting positrons more than the electrons. A possible cause of this could be if the dominant CRs, namely protons, generate Alfvén waves of a particular helicity which scatter and therefore trap positrons more efficiently than electrons in the regions characterized by the enhanced photon and gas densities. Alternatively, higher than considered here energies of photons associated with CR sources may reduce significantly the invoked ‘extreme’ values of the model parameters, due to even more severe KN effects and additional (triplet) pair production processes expected to occur in an intense UV radiation field.

We note in this context that the qualitatively similar effects to the ones analyzed here for the case of our Galaxy have been discussed previously for the case of the host galaxy of nearby radio source Centaurus A by Stawarz et al. (2006). The theoretically predicted isotropic, galactic-scale halo of ultrarelativistic e^\pm pairs thereby (with the energy distribution shaped by the KN and γ -ray annihilation processes), and in particular the resulting TeV emission, has been possibly already detected by the HESS instrument (Aharonian et al. 2009b).

We are grateful to Igor V. Moskalenko, Troy A. Porter, and Michał Ostrowski for helpful discussions and their valuable comments to the paper. We also acknowledge Elliott D. Bloom for pointing out the importance of the triplet pair production process. Finally, we thank the anonymous referee for her/his valuable remarks on the manuscript. LS was supported by the Polish Ministry of Science and Higher Education through the project N N203 380336, and also by the Scandinavian NORDITA program on ‘Physics of Relativistic Flows’.

REFERENCES

- Abdo, A. A., et al. 2009, *Physical Review Letters*, 102, 181101
- Adriani, O., et al. 2009, *Nature*, 458, 607
- Aharonian, F. A., & Ambartsumyan, A. S. 1985, *Astrophysics*, 23, 650
- Aharonian, F. A., & Atoyan, A. M. 1991, *Journal of Physics G Nuclear Physics*, 17, 1769
- Aharonian, F. A., Atoyan, A. M., & Voelk, H. J. 1995, *A&A*, 294, L41
- Aharonian, F., et al. 2008, *Physical Review Letters*, 101, 261104
- Aharonian, F., et al. 2009a, arXiv:0905.0105
- Aharonian, F., et al. 2009b, *ApJ*, 695, L40
- Barwick, S. W., et al. 1997, *ApJ*, 482, L191
- Beatty, J. J., et al. 2004, *Physical Review Letters*, 93, 241102
- Belikov, A. V., & Hooper, D. 2009, arXiv:0906.2251
- Blandford, R. D., & Ostriker, J. P. 1978, *ApJ*, 221, L29
- Blandford, R., & Eichler, D. 1987, *Phys. Rep.*, 154, 1
- Blasi, P. 2009, *Physical Review Letters*, 103, 051104
- Blumenthal, G. R., & Gould, R. J. 1970, *Reviews of Modern Physics*, 42, 237
- Boezio, M., et al. 2000, *ApJ*, 532, 653
- Caprioli, D., Blasi, P., & Amato, E. 2009, *MNRAS*, 396, 2065
- Cesarsky, C. J. 1980, *ARA&A*, 18, 289
- Chang, J., et al. 2008, *Nature*, 456, 362
- Cheng, H.-C., Feng, J. L., & Matchev, K. T. 2002, *Physical Review Letters*, 89, 211301
- Cho, J., Lazarian, A., & Vishniac, E. T. 2003, ‘Turbulence and Magnetic Fields in Astrophysics’, 614, 56
- Coppi, P. S., & Blandford, R. D. 1990, *MNRAS*, 245, 453

- Cowsik, R., & Burch, B. 2009, arXiv:0908.3494
- Crutcher, R., Heiles, C., & Troland, T. 2003, ‘Turbulence and Magnetic Fields in Astrophysics’, 614, 155
- Dermer, C. D., & Schlickeiser, R. 1991, *A&A*, 252, 414
- Dermer, C. D., & Atoyan, A. M. 2002, *ApJ*, 568, L81
- Elahi, P. J., Widrow, L. M., & Thacker, R. J. 2009, arXiv:0906.4352
- Golden, R. L., et al. 1994, *ApJ*, 436, 769
- Grasso, D., et al. 2009, *Astroparticle Physics*, 32, 140
- Hauser, M. G., & Dwek, E. 2001, *ARA&A*, 39, 249
- Higdon, J. C., Lingenfelter, R. E., & Rothschild, R. E. 2009, *ApJ*, 698, 350
- Hillas, A. M., *J. Phys. G: Nucl. Part. Phys.* 31, 95
- Hooper, D., & Zurek, K. M. 2009, *Phys. Rev. D*, 79, 103529
- Hu, H.-B., Yuan, Q., Wang, B., Fan, C., Zhang, J.-L., & Bi, X.-J. 2009, *ApJ*, 700, L170
- Jungman, G., Kamionkowski, M., & Griest, K. 1996, *Phys. Rep.*, 267, 195
- Kardashev, N. S. 1962, *Soviet Astronomy*, 6, 317
- Kelner, S. R., Aharonian, F. A., & Bugayov, V. V. 2006, *Phys. Rev. D*, 74, 034018
- Kobayashi, T., Komori, Y., Yoshida, K., & Nishimura, J. 2004, *ApJ*, 601, 340
- Kulsrud, R., & Pearce, W. P. 1969, *ApJ*, 156, 445
- Kusunose, M., & Takahara, F. 2005, *ApJ*, 621, 285
- Lerche, I. 1967, *ApJ*, 147, 689
- Mastichiadis, A. 1991, *MNRAS*, 253, 235
- Mastichiadis, A., Marscher, A. P., & Brecher, K. 1986, *ApJ*, 300, 178
- Mastichiadis, A., Protheroe, R. J., & Stephens, S. A. 1991, *Proceedings of the Astronomical Society of Australia*, 9, 115
- Moderski, R., Sikora, M., Coppi, P. S., & Aharonian, F. 2005, *MNRAS*, 363, 954

- Moskalenko, I. V., & Strong, A. W. 1998, *ApJ*, 493, 694
- Moskalenko, I. V., & Strong, A. W. 2000, *ApJ*, 528, 357
- Moskalenko, I. V., Strong, A. W., Ormes, J. F., & Potgieter, M. S. 2002, *ApJ*, 565, 280
- Moskalenko, I. V., Strong, A. W., Mashnik, S. G., & Ormes, J. F. 2003, *ApJ*, 586, 1050
- Moskalenko, I. V., Porter, T. A., & Strong, A. W. 2006, *ApJ*, 640, L155
- Nishimura, J., et al. 1980, *ApJ*, 238, 394
- Petrosian, V. 1973, *ApJ*, 186, 291
- Petrosian, V. 2001, *ApJ*, 557, 560
- Petrosian, V., & Liu, S. 2004, *ApJ*, 610, 550
- Pohl, M. 2009, *Phys. Rev. D*, 79, 041301
- Pohl, M., & Esposito, J. A. 1998, *ApJ*, 507, 327
- Porter, T. A., Moskalenko, I. V., & Strong, A. W. 2006, *ApJ*, 648, L29
- Porter, T. A., Moskalenko, I. V., Strong, A. W., Orlando, E., & Bouchet, L. 2008, *ApJ*, 682, 400
- Profumo, S., & Jeltema, T. E. 2009, *Journal of Cosmology and Astro-Particle Physics*, 7, 20
- Ptuskin, V. S., Moskalenko, I. V., Jones, F. C., Strong, A. W., & Zirakashvili, V. N. 2006, *ApJ*, 642, 902
- Schlickeiser, R. 2002, ‘Cosmic Ray Astrophysics’ (Berlin: Springer)
- Shen, C. S. 1970, *ApJ*, 162, L181
- Stawarz, L., Aharonian, F., Wagner, S., & Ostrowski, M. 2006, *MNRAS*, 371, 1705
- Strong, A. W., & Moskalenko, I. V. 1998, *ApJ*, 509, 212
- Strong, A. W., Moskalenko, I. V., & Reimer, O. 2000, *ApJ*, 537, 763
- Strong, A. W., Moskalenko, I. V., & Reimer, O. 2004, *ApJ*, 613, 962
- Strong, A. W., Moskalenko, I. V., & Ptuskin, V. S. 2007, *Annual Review of Nuclear and Particle Science*, 57, 285

Torii, S., et al. 2008, arXiv:0809.0760

Vink, J. 2008, American Institute of Physics Conference Series, 1085, 169

Zdziarski, A. A., & Lightman, A. P. 1985, ApJ, 294, L79

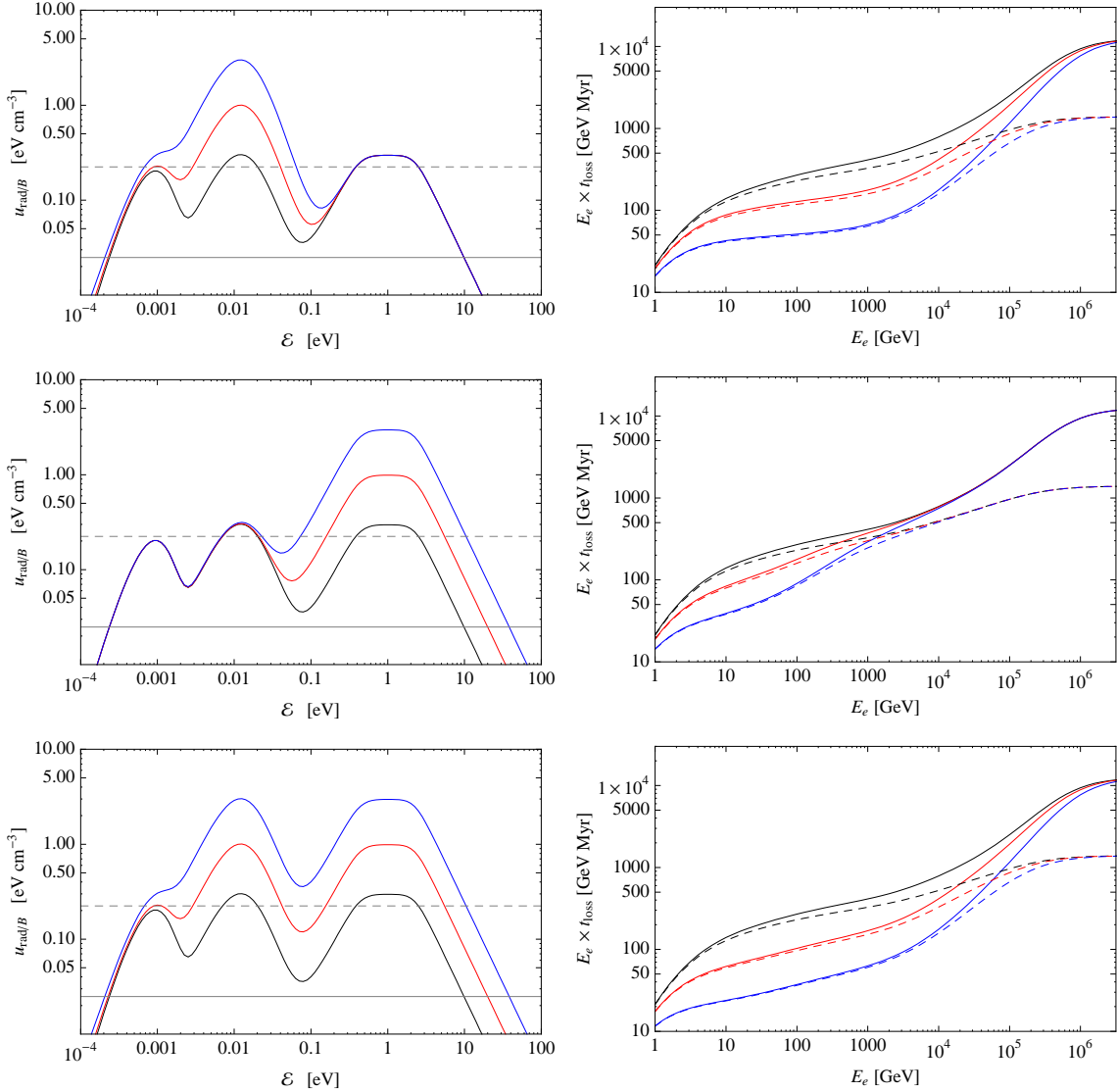


Fig. 1.— **Left panels:** Models of the target photon fields including the CMB and different value of starlight and dust emission. Each panel has three curves for u_{dust} and/or u_{star} equal to 0.3, 1, or 3 eV cm^{-3} , varying independently or together (black, red, and blue curves). In the top panel u_{star} is set as 0.3 eV cm^{-3} . In the middle panel u_{dust} is set as 0.3 eV cm^{-3} . In the bottom panel $u_{\text{star}} = u_{\text{dust}}$. Two different values of the magnetic field densities are also shown: $B = 1 \mu\text{G}$ (solid horizontal lines), and $3 \mu\text{G}$ (dashed horizontal lines). **Right panels:** The energy dependence of the energy losses timescales (multiplied by energy) for the Galactic CR electrons corresponding to the different levels of the Galactic photon and magnetic fields shown on the left panels, and $n_{\text{ism}} = 1 \text{ cm}^{-3}$.

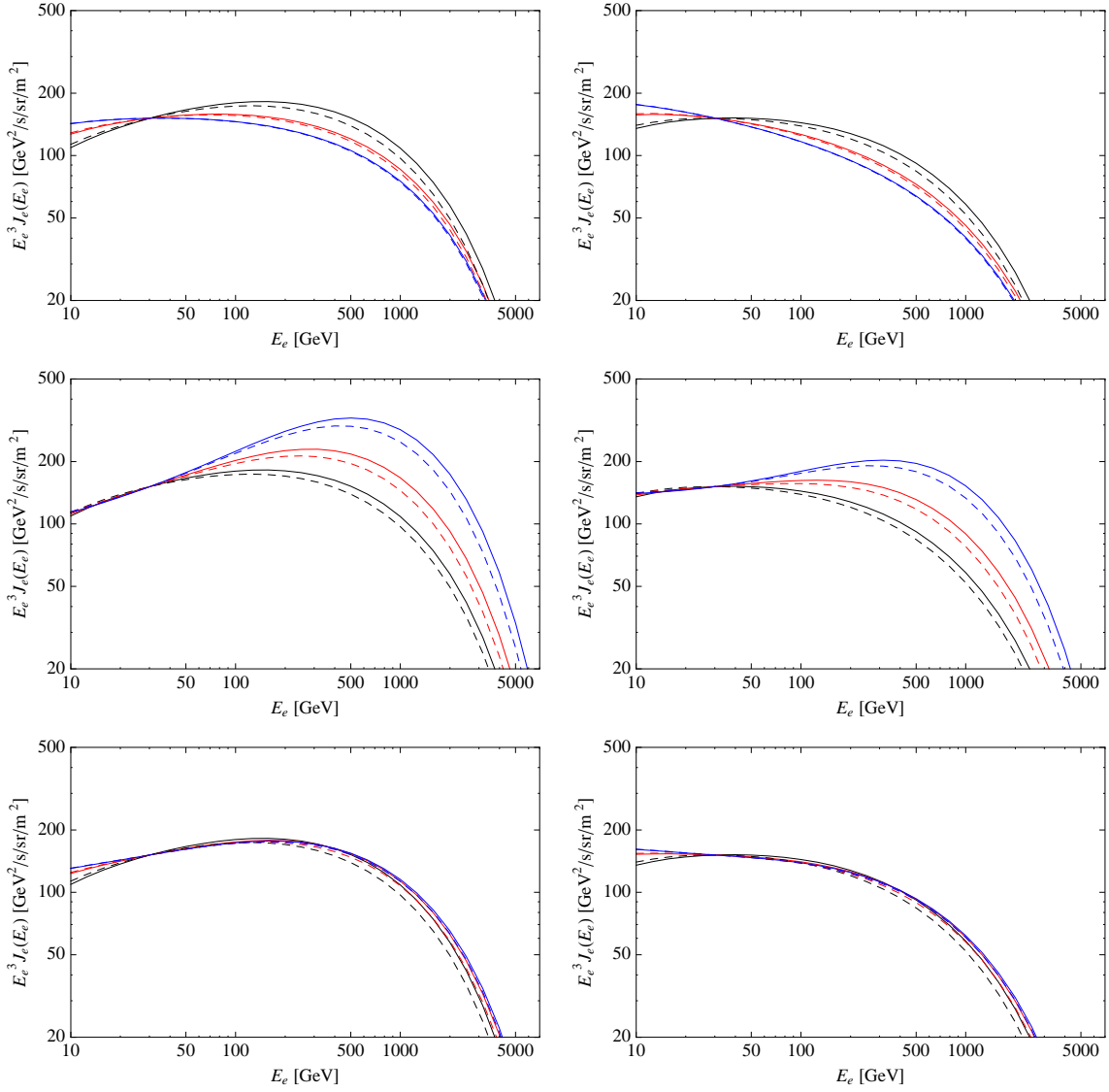


Fig. 2.— The energy spectra of primary electrons corresponding to two different injection spectral indices, $s_e = 2.0$ (left panels) and 2.2 (right panels), for the same set of the model parameters given in Figure 1

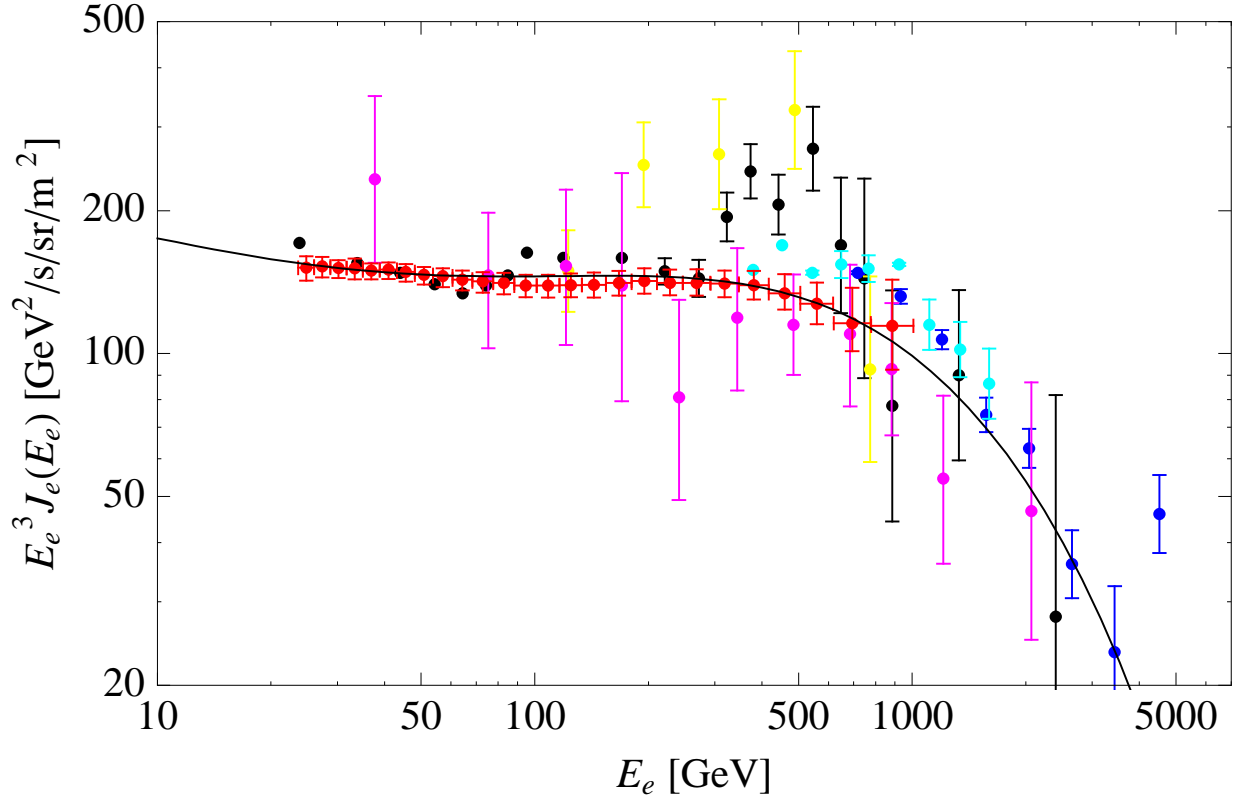


Fig. 3.— Comparison of the observed spectra of the Galactic CR electrons with model spectra calculated for $u_{star} = 3 \text{ eV cm}^{-3}$, $n_{ism} = 1 \text{ cm}^{-3}$, $u_{dust} = 0.1 \text{ eV cm}^{-3}$, $B = 3 \mu\text{G}$, $\ell = 3 \text{ kpc}$, $s_e = 2.42$ and $E_{e,max} = 2.75 \text{ TeV}$. The black solid line corresponds to the energy spectrum of the primary CR electrons calculated using equations (4-7). The data points correspond to different measurements by ATIC (black; Chang et al. 2008), PPB-BETS (yellow; Torii et al. 2008), emulsion chambers (magenta; Kobayashi et al. 2004), HESS (blue and cyan; Aharonian et al. 2008, 2009a, respectively), and Fermi (red; Abdo et al. 2009).

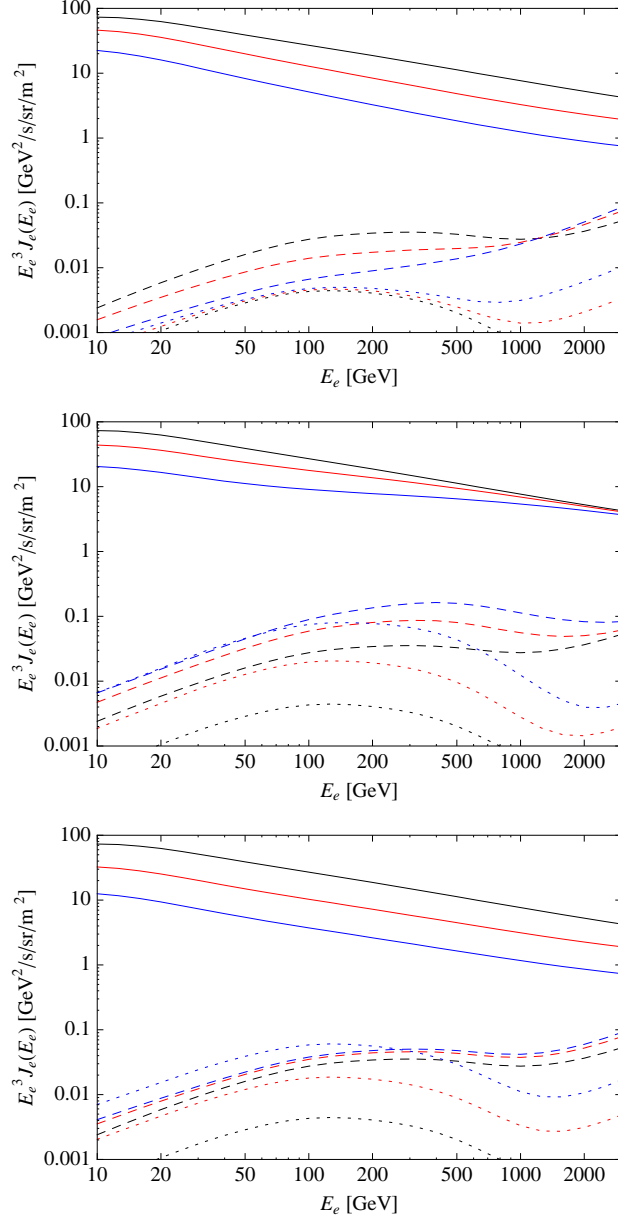


Fig. 4.— The energy spectra of secondary leptons produced in proton-proton collisions (solid lines), and of tertiary pairs produced via absorption of high-energy γ -rays generated in either hadronic or leptonic processes (dashed and dotted lines, respectively), for the same set of the model free parameters as given in Figure 1 (black, red, and blue curves on different panels), except for the single value of the magnetic field $B = 1 \mu\text{G}$.

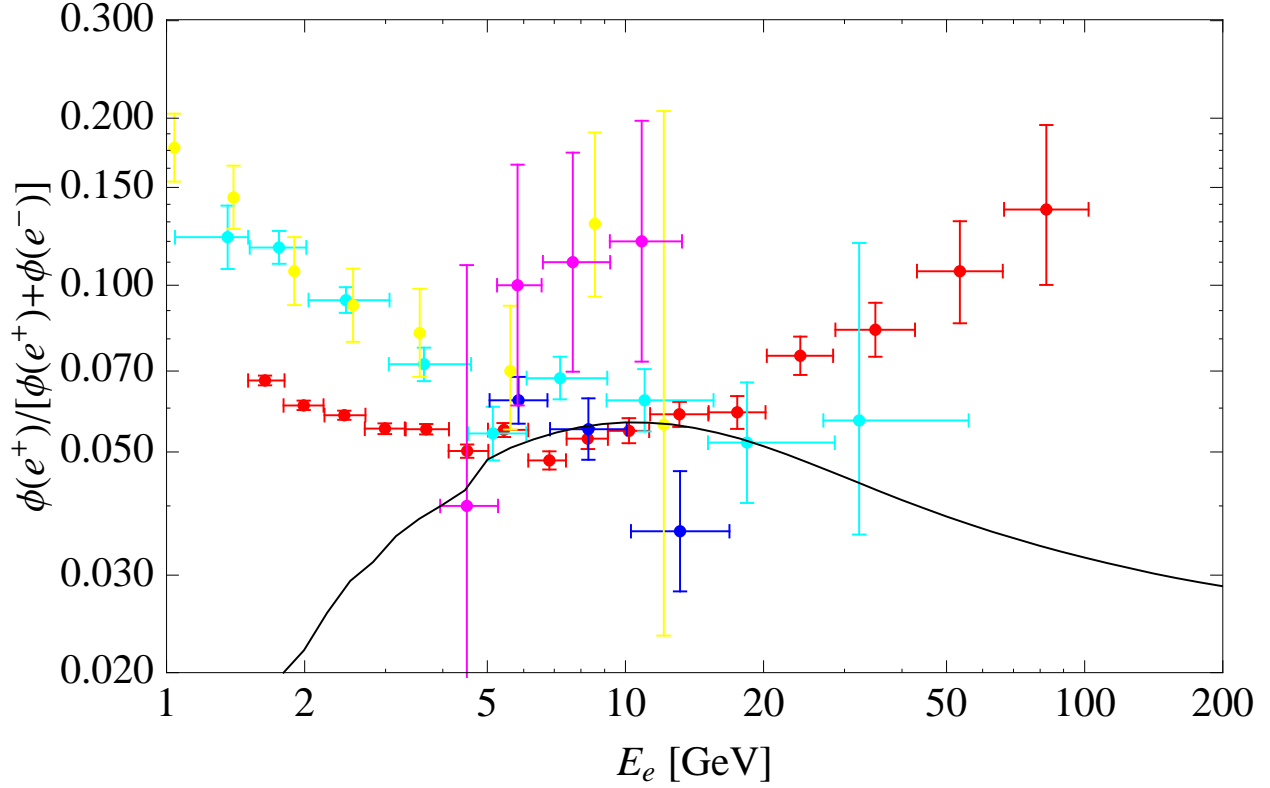


Fig. 5.— The positron-to-electron ratio from different measurements by PAMELA (red symbols; Adriani et al. 2009), HEAT (cyan and blue symbols; Barwick et al. 1997; Beatty et al. 2004), CAPRICE (yellow symbols; Boezio et al. 2000), and imaging calorimeter (magenta symbols; Golden et al. 1994), compared with the model result (line) for the same model parameters as considered in Figure 3, namely $u_{star} = 3 \text{ eV cm}^{-3}$, $n_{ism} = 1 \text{ cm}^{-3}$, $u_{dust} = 0.1 \text{ eV cm}^{-3}$, $B = 3 \mu\text{G}$, $\ell = 3 \text{ kpc}$, $s_e = 2.42$ and $E_{e,max} = 2.75 \text{ TeV}$.

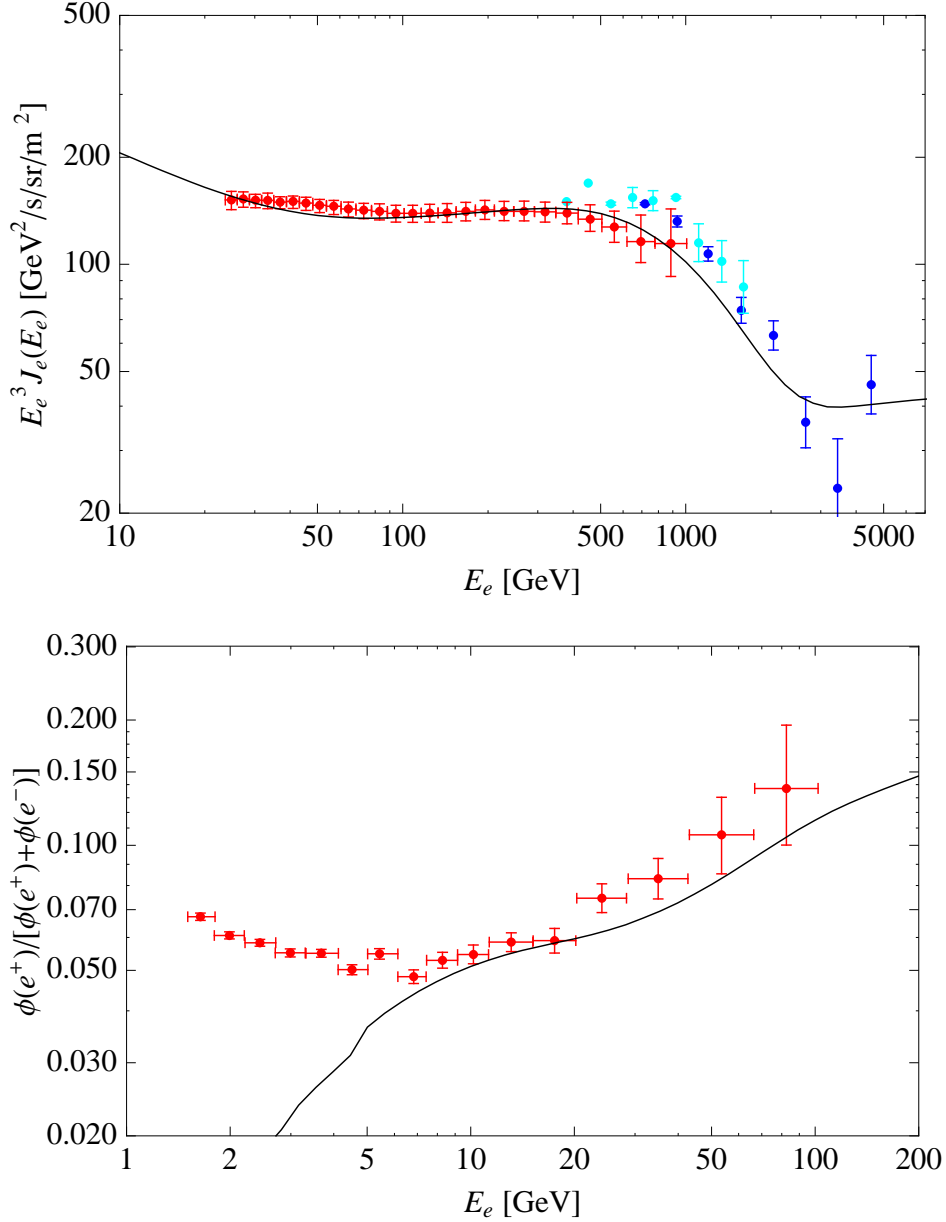


Fig. 6.— **Top panel:** The total energy spectrum of cosmic ray leptons calculated for $u_{star} = 300 \text{ eV cm}^{-3}$, $n_{ism} = 80 \text{ cm}^{-3}$, $u_{dust} = 0.1 \text{ eV cm}^{-3}$, $B = 3 \mu\text{G}$, $\ell = 3 \text{ kpc}$, $s_{e, inj} = 2.65$ and $E_{e, max} = 1.55 \text{ TeV}$ (assuming super-exponential cut-off in the electron injection function). The data points correspond to the measurements by HESS (blue and cyan symbols) and Fermi (red symbols). **Bottom panel:** The resulting positron-to-electron ratio compared with the measurements by PAMELA (red symbols).